

# Effect of quintic nonlinearity on self-phase modulation and modulation instability in multiple coupled quantum wells under electromagnetically induced transparency

Rohit Mukherjee\*, S. Konar

*Department of Physics, Birla Institute of Technology, Mesra-835215, Ranchi, India*



## ARTICLE INFO

**Keywords:**  
 Coupled quantum well  
 Electromagnetically induced transparency  
 Self-phase modulation  
 Modulation instability

## ABSTRACT

The self-phase modulation and modulation instability of an optical probe electromagnetic field in multiple quantum well systems under electromagnetically induced transparency has been investigated. The probe field experiences large Kerr and quintic nonlinearities that can be controlled by two controlling laser beams. The probe beam experiences self-phase modulation which is suppressed by the quintic nonlinearity. The probe field is modulationally unstable due to the existence of large nonlinearities. The bandwidth of unstable frequencies and growth of the instability could be controlled by the probe beam power, the Rabi frequency and detunings of two control fields. The presence of the higher order nonlinearity and dispersion significantly reduce the instability growth and bandwidth of unstable frequency.

## Introduction

Recently, significant attention has been paid to quantum coherence and interference effects in semiconductor nanostructures due to applications in optical communications and signal processing [1–4]. Quantum coherent phenomena such as lasing without inversion [5], coherent population trapping [6], electromagnetically induced transparency (EIT) [7,8], slow and fast light [9–11], soliton propagation [10] etc., have been investigated both theoretically as well as experimentally. Particularly, due to important applications significant attention has been paid to the investigation of the EIT in semiconductor nanostructures [7,8]. The magnitude of Kerr nonlinearity and linear absorption can be controlled by quantum coherence in quantum wells (QWs). In addition, large optical nonlinearity can be engineered in QWs due to quantum coherence. The EIT enhanced third order susceptibility and its role in determining the dynamics of optical solitons, all optical switching, four wave mixing etc; have been investigated in QW nanostructures as well as in atomic systems [6,7,9–11]. By virtue of quantum coherence and interference effects, QWs not only possess enhanced Kerr nonlinearity, it can possess significant higher order nonlinearity as well, particularly quintic nonlinearity [7,12–15].

Although the existence of the enhanced Kerr nonlinearity in semiconductor quantum wells (SQWs) in the regime of EIT has been known for some time [16–18], existence of large quintic nonlinearity has been predicted very recently [11,16,19,20]. Materials that exhibit significant

quintic nonlinearity plays important role in quantum information network such as quantum memory of light [3,4], generation of correlated photon pairs [4], and 3-qubit quantum processing [1,21]. The phase noise can be reduced by quintic nonlinearity and hence the performance of interferometry can be improved [22], and consequently quintic nonlinearity can improve high precession measurements [23]. New phenomena such as liquid light condensate [24], transverse pattern and stable 2D solitons can be observed in materials that exhibit large quintic nonlinearity. Despite extensive investigations on the Kerr nonlinearity, barring a few, higher order nonlinearities such as quintic nonlinearity have not received adequate attention in quantum wells, particularly in multiple double quantum wells. Recently, modulation instability was examined [18] in a three level quantum well system incorporating quintic nonlinearity. Roles of quintic nonlinearity and control field detuning were examined. Along this line, in this communication, we plan to investigate the existence of fifth order nonlinearity in the regime of electromagnetically induced transparency in multiple asymmetric double quantum well systems. We also plan to examine self-phase modulation of short pulses, and modulation instability of a quasi-continuous or continuous wave probe beam in these systems.

The arrangement of the article is as follows: The theoretical model of the quantum well is presented and the expressions for susceptibilities have been derived in section 2. The dynamical equation of the propagating probe has been derived in section 3. In section 4, we investigate properties of linear, Kerr and quintic nonlinearities. The phenomena of

\* Corresponding author.

E-mail address: [phdap10002.18@bitmesra.ac.in](mailto:phdap10002.18@bitmesra.ac.in) (R. Mukherjee).

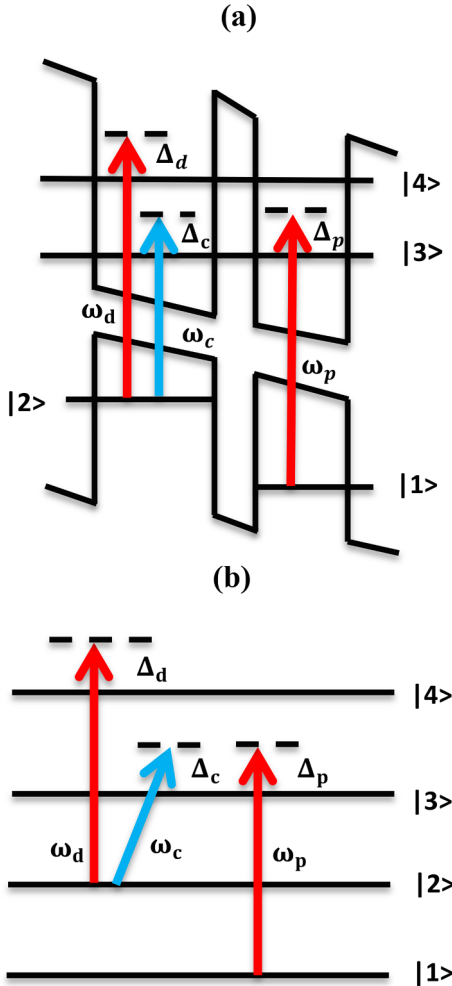


**Fig. 1.** (a) Schematic energy level diagram, and (b) N-type excitation scheme of the asymmetric quantum well. Levels  $|1\rangle$  and  $|2\rangle$  are localized hole states, whereas levels  $|3\rangle$  and  $|4\rangle$  are delocalized bonding and anti-bonding electronic states.

self-phase modulation (SPM) and modulation instability (MI) have been discussed in section 5 and 6, respectively. An abridged conclusion has been added in section 7.

#### Description of asymmetric coupled quantum wells and governing equations

We consider 200 periods of double quantum wells (QW), each period consists of a wide well (WW) and a narrow well (NW), as shown in Fig. 1. Each narrow well is 35 monolayer (100 Å) thick, while each wide well is 51 monolayer (145 Å) thick, and these two wells are separated by 9 monolayer (25 Å) thick Al<sub>0.2</sub>Ga<sub>0.8</sub>As barrier [25,26]. The monolayer in the wide and narrow well is made of GaAs material with electron density  $10^{11}$  cm<sup>-2</sup> and has thickness 2.83 Å. These double quantum wells are separated from each other by a 200 Å wide Al<sub>0.2</sub>Ga<sub>0.8</sub>As barrier. Energy levels  $|1\rangle$  and  $|2\rangle$  in the valence band are localized hole states. Energy levels  $|3\rangle$  and  $|4\rangle$  are the bonding and antibonding states of electrons which arise as a result of strongly coherent coupling between electronic wave-functions in the two wells through thin barrier. In this configuration, a continuous wave (CW) or quasi-continuous probe beam with angular frequency  $\omega_p$  and amplitude  $E_p$  couples the transition from energy level  $|1\rangle$  to  $|3\rangle$ . A control beam of angular frequency  $\omega_c$  and amplitude  $E_c$  couples the transition from energy level  $|2\rangle$  to  $|3\rangle$ , while a second control beam of angular frequency  $\omega_d$  and amplitude  $E_d$  couples the transition from energy level

$|2\rangle$  to  $|4\rangle$ . The electric fields of the probe and control beams can be written as,

$$\vec{E} = \sum_{i=p,c,d} \hat{e}_i \vec{E}_i \exp\{i(k_i z - \omega_i t)\} + c. c. , \quad (1)$$

where,  $\hat{e}_p$ ,  $\hat{e}_c$  and  $\hat{e}_d$  are unit vectors along the polarization directions of the probe ( $E_p$ ) and control fields  $E_c$  and  $E_d$ , respectively. Here,  $k_p$ ,  $k_c$  and  $k_d$  are the wave vectors of the probe and two control beams, respectively, whereas the c.c term signifies complex conjugate. In the Schrödinger picture, the semiclassical Hamiltonian describing the system of electrons and the fields can be written as,

$$\hat{H} = \hat{H}_0 + \hat{H}_1 \quad (2)$$

where,  $\hat{H}_0$  is the unperturbed Hamiltonian without any field and  $\hat{H}_1$  describes the interaction between electrons of coupled quantum wells and the applied fields. Under the rotating wave approximation [21], these two Hamiltonians can be written as,

$$\hat{H}_0 = E_1 |1\rangle\langle 1| + E_2 |2\rangle\langle 2| + E_3 |3\rangle\langle 3| + E_4 |4\rangle\langle 4|, \quad (3)$$

and

$$\begin{aligned} \hat{H}_1 &= -\hbar\{\Omega_p \exp(i(k_p z - \omega_p t)) |3\rangle\langle 1| + \Omega_c \exp(i(k_c z - \omega_c t)) |3\rangle\langle 2| \\ &\quad + \Omega_d \exp(i(k_d z - \omega_d t)) |4\rangle\langle 2| + h. c\} \end{aligned} \quad (4)$$

where, the Rabi-frequencies of the probe and two control fields are defined as,  $\Omega_p = \frac{\mu_{13} \cdot \hat{e}_p E_p}{\hbar}$ ,  $\Omega_c = \frac{\mu_{23} \cdot \hat{e}_c E_c}{\hbar}$  and  $\Omega_d = \frac{\mu_{24} \cdot \hat{e}_d E_d}{\hbar}$ , respectively; and h.c signifies hermitian conjugate. The parameter  $\mu_{ij}$  ( $= \langle i | e_z | j \rangle$ ) is the dipole moment of the transition between energy levels  $|i\rangle$  and  $|j\rangle$ . The state vectors of the system in the Schrödinger picture can be written as,

$$|\psi_s(t)\rangle = \sum_{j=1}^4 C_j(t) |j\rangle, \quad (5)$$

where,  $|j\rangle$  is the eigenstate of unperturbed Hamiltonian and  $C_j(t)$  is the time dependent normalized probability amplitude of finding the electron in the subband  $|j\rangle$ . The wave function in the interaction picture can be easily obtained as,

$$\begin{aligned} |\psi_{int}\rangle &= C_1(t) \exp\left(\frac{iE_1 t}{\hbar}\right) |1\rangle + C_2(t) \exp\left(\frac{iE_2 t}{\hbar}\right) |2\rangle + C_3 \\ &\quad (t) \exp\left(\frac{iE_3 t}{\hbar}\right) |3\rangle + C_4(t) \exp\left(\frac{iE_4 t}{\hbar}\right) |4\rangle. \end{aligned} \quad (6)$$

The interaction picture Hamiltonian can be written as,

$$\begin{aligned} \hat{H}_{int} &= \Omega_p \exp(i(k_p z - \omega_p t)) |3\rangle\langle 1| \\ &\quad \exp\left(\frac{i(E_3 - E_1)}{\hbar}\right) + \Omega_c \exp(i(k_c z - \omega_c t)) |3\rangle\langle 2| \exp\left(\frac{i(E_3 - E_2)}{\hbar}\right) + \Omega_d \\ &\quad \exp(i(k_d z - \omega_d t)) |4\rangle\langle 2| \exp\left(\frac{i(E_4 - E_2)}{\hbar}\right) + h. c \end{aligned} \quad (7)$$

By virtue of the use of Schrödinger equation in interacting picture, we can easily obtain equations of probability amplitudes which are as follows,

$$\dot{A}_1 = i A_3 \Omega_p^*, \quad (8)$$

$$\dot{A}_2 = i(\Delta_p - \Delta_c) A_2 + i(A_3 \Omega_c^* + A_4 \Omega_d^*) - \gamma_2 A_2, \quad (9)$$

$$\dot{A}_3 = i A_3 \Delta_p + i(A_1 \Omega_p + A_2 \Omega_c) - \gamma_3 A_3, \quad (10)$$

$$\dot{A}_4 = i(\Delta_p - \Delta_c + \Delta_d) A_4 + i \Omega_d A_2 - \gamma_4 A_4, \quad (11)$$

where, the dot over the probability amplitude  $A_j$  represents derivative w.r.t time. Here, the detuning frequencies associated with these fields are defined as,  $\Delta_p = \omega_p - \frac{E_3 - E_1}{\hbar}$ ,  $\Delta_c = \omega_c - \frac{E_3 - E_2}{\hbar}$  and  $\Delta_d = \omega_d - \frac{E_4 - E_2}{\hbar}$ , respectively. In writing above, we have introduced the transformation,  $C_j(t) = A_j(t) \exp\left(i\left\{k_j z - \left(\frac{E_k}{\hbar} + \lambda_k\right)t\right\}\right)$  where,  $k_1 = 0$ ,  $k_2 = k_p - k_c$ ,  $k_3 = k_p$ ,  $k_4 = k_p - k_c + k_d$ ,  $\lambda_1 = 0$ ,  $\lambda_2 = \Delta_p - \Delta_c$ ,  $\lambda_3 = \Delta_p$ ,  $\lambda_4 = \Delta_p - \Delta_c + \Delta_d$ . The total population decay rate in the sub-band  $|j| > 1$  is  $\gamma_j = \gamma_{jl} + \gamma_j^{dph}$ , which consists of a population decay term ( $\gamma_j$ ) due to longitudinal optical phonon emission at low temperature, and dephasing term ( $\gamma_j^{dph}$ ) originates from electron-electron, electron-phonon scattering at the interfaces. In the present investigation, the population decay rates ( $\gamma_2$ ,  $\gamma_3$ ,  $\gamma_4$ ) from different energy levels are chosen phenomenologically.

In the present context, the probe beam is sufficiently weak in comparison to the control beams i.e.,  $\Omega_p \ll \Omega_c$  and  $\Omega_d$ , hence, due to quantum interference effect, the carrier density in the ground state is not too much depleted [9] i.e.,  $A_1 \approx 1$ ,  $A_2 = A_3 = 0$ ,  $t > 0$ . Now, we assume that,  $A_j = \sum_k A_j^{(k)}$ , where,  $A_j^{(k)}$  is k-th order perturbation of  $A_j$ . Under the regime of adiabatic formulation [27], it can be shown that  $A_j^{(0)} = \delta_{j1}$  and  $A_j^{(1)} = 0$ , where,  $\delta_{j1}$  is Kroncker delta function. By virtue of above approximation, Eqs. (9)–(11) reduce to,

$$\frac{d}{dt}A_2^{(1)} = i(\Delta_p - \Delta_c)A_2^{(1)} + i(A_3^{(1)}\Omega_c^* + A_4^{(1)}\Omega_d^*) - \gamma_2 A_2^{(1)}, \quad (12)$$

$$\frac{d}{dt}A_3^{(1)} = i\Delta_p A_3^{(1)} + i(\Omega_p + \Omega_c A_2^{(1)}) - \gamma_3 A_3^{(1)}, \quad (13)$$

$$\frac{d}{dt}A_4^{(1)} = i(\Delta_p - \Delta_c + \Delta_d)A_4^{(1)} + i\Omega_d A_2^{(1)} - \gamma_4 A_4^{(1)}. \quad (14)$$

Introducing Fourier transformation of Eqs. (12)–(14) we get,

$$(\omega + \Delta_p - \Delta_c + i\gamma_2)\alpha_2^{(1)} + \Omega_c^*\alpha_3^{(1)} + \Omega_d^*\alpha_4^{(1)} = 0, \quad (15)$$

$$\Omega_c\alpha_2^{(1)} + (\omega + \Delta_p + i\gamma_3)\alpha_3^{(1)} = -\Lambda_p, \quad (16)$$

$$\Omega_d\alpha_2^{(1)} + (\omega + \Delta_p - \Delta_c + \Delta_d + i\gamma_4)\alpha_4^{(1)} = 0, \quad (17)$$

where,  $\alpha_j^{(1)}$  and  $\Lambda_p$  are Fourier transformation of  $A_j^{(1)}$  and  $\Omega_p$  respectively,  $\omega$  is the Fourier transform variable. After some simple algebra we easily get,  $\alpha_2^{(1)} = \frac{\Omega_c^*Z(\omega)}{D(\omega)}\Lambda_p$ ,  $\alpha_3^{(1)} = -\frac{D_p(\omega)}{D(\omega)}\Lambda_p$ ,  $\alpha_4^{(1)} = \frac{\Omega_d^*\Omega_d}{D(\omega)}\Lambda_p$ . Application of inverse Fourier transformation of  $\alpha_2^{(1)}$ ,  $\alpha_3^{(1)}$ ,  $\alpha_4^{(1)}$  leads to  $A_2^{(1)} = \frac{\Omega_c^*Z(0)}{D(0)}\Omega_p$ ,  $A_3^{(1)} = -\frac{D_p(0)}{D(0)}\Omega_p$ ,  $A_4^{(1)} = \frac{\Omega_d^*\Omega_d}{D(0)}\Omega_p$ ; where,  $D(\omega) = \{X(\omega)Y(\omega)Z(\omega) - |\Omega_d|^2 Y(\omega) - |\Omega_c|^2 Z(\omega)\}$ ,  $D_p(\omega) = \{X(\omega)Z(\omega) - |\Omega_d|^2\}$ ,  $X(\omega) = (\omega + \Delta_p - \Delta_c + i\gamma_2)$ ,  $Y(\omega) = (\omega + \Delta_p + i\gamma_3)$ , and  $Z(\omega) = (\omega + \Delta_p - \Delta_c + \Delta_d + i\gamma_4)$ .

Using Maxwell's wave equation and employing slowly varying envelope approximation [9], the amplitude of the propagating probe beam along the z-direction can be easily obtained which is as follows:

$$\frac{\partial \Omega_p}{\partial z} + \frac{1}{c} \frac{\partial \Omega_p}{\partial t} = iK_{13}A_3^{(1)} + (NLT)A_3^{(1)}, \quad (18)$$

where,  $K_{13} = \frac{N|\mu_{13}|^2}{2\hbar\epsilon_0 c}\omega_p$ ;  $c$  and  $\epsilon_0$  are the speed of light in vacuum and permittivity of free space, respectively,  $\hbar$  is reduced Planck's constant. Here,  $N$  is the electron density and the nonlinear term (NLT) is expressed as,

$$NLT = -iK_{13}[\{|A_2^{(1)}|^2 + |A_3^{(1)}|^2 + |A_4^{(1)}|^2\} - \{|A_2^{(1)}|^2 + |A_3^{(1)}|^2 + |A_4^{(1)}|^2\}^2]. \quad (19)$$

The induced polarization  $\vec{P}$  around the probe frequency  $\omega_p$  can be written as,  $\vec{P}(\omega_p) = \epsilon_0\chi_p(\omega_p)E_p$ , where the susceptibility  $\chi_p(\omega_p)$  at the probe frequency is expressed as a summation of linear and higher order nonlinear terms i.e.,

$$\chi_p = \chi^{(1)} + \chi^{(3)}|E_p|^2 + \chi^{(5)}|E_p|^4 + \dots, \quad (20)$$

The linear and nonlinear susceptibilities, after some mathematical calculation from Eqs. (18)–(20), are obtained as follows:

$$\chi^{(1)} = -\frac{2cK_{13}}{\omega_p} \frac{D_p(0)}{D(0)}, \quad (21)$$

$$\chi^{(3)} = \frac{2c|\mu_{13}|^2 K_{13}}{\omega_p \hbar^2} \left( \frac{(|\Omega_c Z(0)|^2 + |D_p(0)|^2 + |\Omega_c \Omega_d|^2)}{|D(0)|^2} \right) \frac{D_p(0)}{D(0)}, \quad (22)$$

and

$$\chi^{(5)} = -\frac{2c|\mu_{13}|^4 K_{13}}{\omega_p \hbar^4} \left( \frac{(|\Omega_c Z(0)|^2 + |D_p(0)|^2 + |\Omega_c \Omega_d|^2)}{|D(0)|^2} \right)^2 \frac{D_p(0)}{D(0)}. \quad (23)$$

We have derived only upto quintic terms since further higher order terms are insignificant. In the next section, we have examined the behavior of linear and nonlinear susceptibilities.

### Nonlinear Schrödinger equation of the probe field

To investigate the dispersion experienced by the probe beam in the multiple double QWs, we begin with the Fourier transformation of the linearized version of Eq. (18) which turns out to be:

$$\frac{\partial \Lambda_p}{\partial z} - i\Gamma(\omega)\Lambda_p = 0, \quad (24)$$

where, the parameter  $\Gamma(\omega) = \frac{\omega}{c} - K_{13} \frac{D_p(\omega)}{D(\omega)}$  can be identified as frequency dependent propagation constant. The solution of Eq. (24) can be immediately obtained as:

$$\Lambda_p(z, \omega) = \Lambda_p(0, \omega) \exp(i\Gamma(\omega)z). \quad (25)$$

The parameter  $\Gamma(\omega)$  has been expanded around the probe central frequency (i.e.,  $= 0$ ) as:

$$\Gamma(\omega) = \Gamma(0) + \Gamma_1(0)\omega + \frac{1}{2!}\omega^2\Gamma_2(0) + \frac{1}{3!}\omega^3\Gamma_3(0) + \frac{1}{4!}\omega^4\Gamma_4(0) + \dots, \quad (26)$$

where,  $\Gamma_n(0) = \frac{d^n\Gamma(\omega)}{d\omega^n}|_{\omega=0}$ ; the parameter  $\Gamma(0) = \phi + i\frac{\beta}{2}$ , where  $\phi$  and  $\beta$  represent the rate of the phase shift and linearized absorption of the probe beam, respectively.  $\Gamma_1(0)$  is related to group velocity  $v_g (= Re(1/\Gamma_1(0)))$  of the probe beam. The parameter  $\Gamma_2(0)$  describes the group velocity dispersion (GVD) of the probe field. Likewise  $\Gamma_3$  and  $\Gamma_4$  are third and fourth order dispersion, respectively.

Here,

$$\Gamma(0) = -K_{13} \frac{D_p(0)}{D(0)} \quad (27)$$

$$\Gamma_1(0) = \frac{1}{c} - K_{13} \frac{A(0)}{D(0)} + K_{13} D_p(0) \left( \frac{D_p(0) + Y(0)Z(0) + Z(0)X(0)}{|D(0)|^2} \right) \quad (28)$$

$$\Gamma_2(0) = -\frac{2K_{13}}{D(0)} + 2K_{13} \frac{(2\Delta_p - \Delta_c + i\gamma_2 + i\gamma_3)D_{11}(0)}{|D(0)|^2} - 2K_{13}D_p(0) \left( \frac{|D_{11}(0)|^2}{|D(0)|^3} + K_{13}D_p(0) \frac{D_{22}(0)}{|D(0)|^2} \right), \quad (29)$$

$$\Gamma_3(0) = \frac{6K_{13}D_{11}(0)}{|D(0)|^2} - 6K_{13} \frac{|D_{11}(0)|^2}{|D(0)|^3} + 3K_{13} \frac{A(0)D_{22}(0)}{|D(0)|^2} + 6K_{13}D_p(0) \left( \frac{|D_{11}(0)|^3}{|D(0)|^4} + \frac{6K_{13}D_p(0)}{|D(0)|^2} - 6K_{13}D_p(0) \frac{D_{11}(0)D_{22}(0)}{|D(0)|^3} \right) \quad (30)$$

$$\begin{aligned} \Gamma_4(0) = & -24K_{13}\frac{[D_{11}(0)]^2}{[D(0)]^3} + 12K_{13}\frac{D_{22}(0)}{[D(0)]^2} + 24K_{13}\frac{A(0)[D_{11}(0)]^3}{[D(0)]^4} - 24K_{13} \\ & \frac{A(0)D_{22}(0)D_{11}(0)}{[D(0)]^3} + 24K_{13}\frac{A(0)}{[D(0)]^2} - 24K_{13}D_p(0)\frac{[D_{11}(0)]^4}{[D(0)]^5} + 36 \\ & K_{13}D_p(0)\frac{D_{22}(0)[D_{11}(0)]^2}{[D(0)]^4} - 6K_{13}D_p(0)\frac{D_{22}(0)}{[D(0)]^3} - 48K_{13} \\ & D_p(0)\frac{D_{11}(0)}{[D(0)]^3} \end{aligned} \quad (31)$$

$$A(\omega) = (\omega + 2\Delta_p - \Delta_c + i\gamma_2 + i\gamma_3), \quad (32)$$

$$D_{11}(\omega) = \{\omega + Y(\omega)Z(\omega) + Z(\omega)X(\omega) + D_p(\omega) - |\Omega_c|^2\}, \quad (33)$$

$$D_{22}(\omega) = (\omega + 6\Delta_p + 2\Delta_d - 4\Delta_c + 2i\gamma_2 + 2i\gamma_3 + 2i\gamma_4). \quad (34)$$

The linearized Eq. (24) has been derived ignoring optical nonlinearities of the probe field. To investigate nonlinear propagation dynamics, we need to incorporate linear as well as nonlinear terms. These nonlinear terms are responsible for several interesting phenomena such as self-phase modulation, modulation instability, soliton propagation, supercontinuum generation etc. Thus, to investigate nonlinear dynamics of optical beams or pulses, instead of examining Eq. (24) further, we pick up nonlinear Eq. (18) which can be recasted in the following form:

$$\frac{\partial \Lambda_p}{\partial z} - i\Gamma(\omega)\Lambda_p - (NLT)A_3^{(1)} = 0. \quad (35)$$

It is obvious that Eq. (24) can be recovered from Eq. (35) by ignoring nonlinear terms. To proceed further, we adopt the procedure developed by Wu and Deng [28,29], insert  $\Gamma(\omega)$  from Eq. (26) in Eq. (35), and keep terms upto  $\omega^4$ , and finally obtain following equation:

$$\begin{aligned} & \left\{ \frac{\partial}{\partial z} + i\Gamma_1(0)\omega - i\Gamma_2(0)\frac{\omega^2}{2!} - i\Gamma_3(0)\frac{\omega^3}{3!} + \Gamma_4(0)\frac{\omega^4}{4!} \right\} \Lambda_p \exp(i\Gamma(0)\omega) \\ & = iK_{13}\frac{D_p(\omega)}{D(\omega)}\Lambda_p(0, \omega) \exp(i\Gamma(\omega)z)[|A_2^{(1)}|^2 + |A_3^{(1)}|^2 + |A_4^{(1)}|^2] \\ & - [|A_2^{(1)}|^2 + |A_3^{(1)}|^2 + |A_4^{(1)}|^2]^2. \end{aligned} \quad (36)$$

By virtue of inverse Fourier transformation of Eq. (36) and employing values of  $A_2^{(1)}$ ,  $A_3^{(1)}$ ,  $A_4^{(1)}$ , we immediately obtain,

$$\begin{aligned} & i\frac{\partial \Omega_p}{\partial z} + i\Gamma_1(0)\frac{\partial \Omega_p}{\partial t} - \frac{1}{2!}\Gamma_2(0)\frac{\partial^2 \Omega_p}{\partial t^2} - \frac{i}{3!}\Gamma_3(0)\frac{\partial^3 \Omega_p}{\partial t^3} + \frac{1}{4!}\Gamma_4 \\ & (0)\frac{\partial^4 \Omega_p}{\partial t^4} + \frac{\omega_p \hbar^2}{2c |\mu_{31}|^2} \chi^{(3)} |\Omega_p|^2 \Omega_p \exp(-\beta z) + \frac{\omega_p \hbar^4}{2c |\mu_{31}|^4} \chi^{(5)} |\Omega_p|^4 \Omega_p \\ & \exp(-2\beta z) = 0. \end{aligned} \quad (37)$$

With the introduction of a moving frame defined by  $z = \xi$ ,  $T = t - \frac{z}{v_g}$ , Eq. (37) can be rewritten as:

$$\begin{aligned} & i\frac{\partial A}{\partial \xi} - \frac{1}{2!}\Gamma_2(0)\frac{\partial^2 A}{\partial T^2} - \frac{i}{3!}\Gamma_3(0)\frac{\partial^3 A}{\partial T^3} + \frac{1}{4!}\Gamma_4(0)\frac{\partial^4 A}{\partial T^4} + \gamma |A|^2 A \exp \\ & (-\beta \xi) + \delta |A|^4 A \exp(-2\beta \xi) = 0, \end{aligned} \quad (38)$$

where, the normalized envelope of the probe beam  $A = \frac{\hbar \Omega_p}{\mu_{13}} \left( \frac{n_0 c \epsilon_0 S}{2} \right)^{\frac{1}{2}}$ .  $\gamma = \frac{\omega_p}{n_0 c^2 \epsilon_0 S} \chi^{(3)}$ , and  $\delta = \frac{2\omega_p}{n_0^2 c^3 \epsilon_0^2 S^2} \chi^{(5)}$  are two nonlinear coefficients. Here,  $n_0$ ,  $S$  are respectively the linear refractive index of the system and cross section area of the probe beam. Eq. (38) is the modified nonlinear Schrödinger equation which predicts the nonlinear evolution of the probe beam inside the multiple double QW system. Since the further investigation shall be in the regime of EIT window where absorption is insignificant, we can safely assume  $\beta \approx 0$  and  $\exp(-\beta \xi) \approx \exp(-2\beta \xi) \approx 1$  in further discussion.

### Linear and nonlinear susceptibilities

In this section, we examine linear, Kerr and quintic nonlinearities of the multiple double quantum well system considered in the present

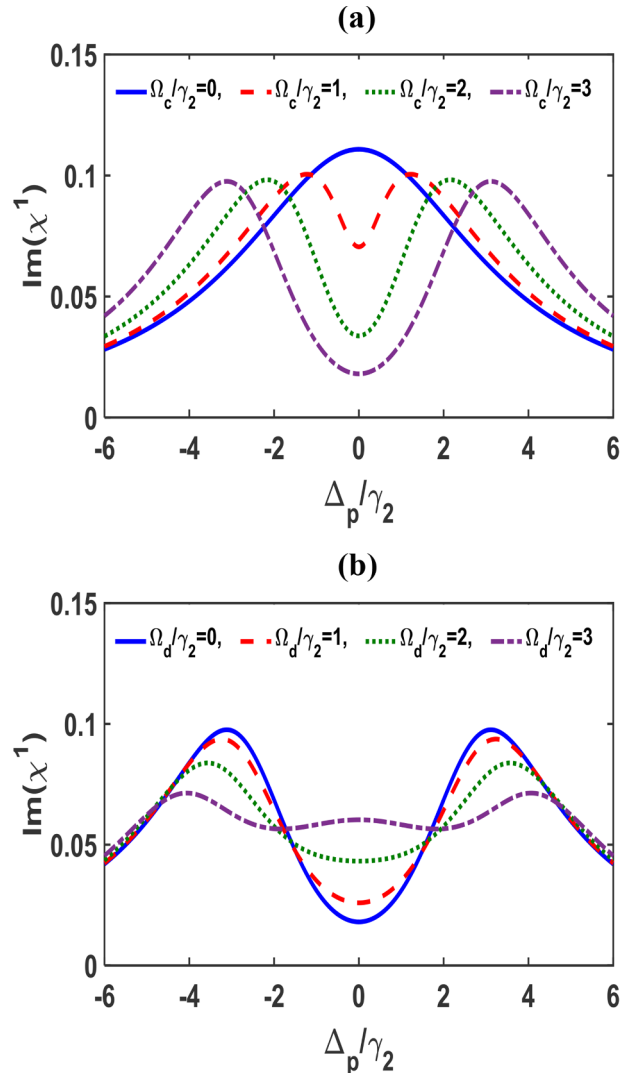


**Fig. 2.** Variations of imaginary part of the linear susceptibility [ $\text{Im}(\chi^{(1)})$ ] with normalized probe detuning. (a) For different values of the Rabi-frequency of the first control field ( $\Omega_c$ ), while the second control field ( $\Omega_d$ ) is switched off. (b) For different values of the Rabi-frequency of the second control field ( $\Omega_d$ ), while keeping the value of the first control field fixed ( $\Omega_c = 3 \text{ ps}^{-1}$ ). The value of detunings are  $\Delta_c = \Delta_d = 0$ .

communication. To begin with, we first examine the linear susceptibility of the system which shall be useful for subsequent analysis. The relevant physical parameters pertaining to the present system are:  $N = 10^{22} \text{ m}^{-3}$ ,  $\mu_{13} = 26.88 \times 10^{-29} \text{ Cm}$ ,  $\omega_p = 2.537 \times 10^{15} \text{ s}^{-1}$ ,  $K_{13} = 16.4 \times 10^{17} \text{ m}^{-1} \text{s}^{-1}$ ,  $\gamma_2 = 1 \times 10^{12} \text{ s}^{-1}$ , and  $\gamma_3 = \gamma_4 = 7\gamma_2$ . In Fig. 2(a), we have demonstrated the variation of imaginary part of linear susceptibility with the normalized probe detuning ( $\Delta_p$ ) for different values of the Rabi frequency  $\Omega_c$  of the first control field, while the second control field  $\Omega_d$  is turned off. From Fig. 2(a), it is evident that, in absence of the first control field ( $\Omega_c$ ), the probe beam experiences large absorption around  $\Delta_p = 0$ . By increasing value of  $\Omega_c$ , a transparency window is formed, which broadens with the increase in the value of  $\Omega_c$ . This suppression of the absorption of the probe beam is due to the quantum destructive interference effect which is driven by the strong control field and is well understood [7,8]. The variation of  $\text{Im}(\chi^{(1)})$  with  $\Delta_p$  for different values of the  $\Omega_d$  has been demonstrated in Fig. 2(b) while keeping the values of the first control field  $\Omega_c$  is constant. From Fig. 2(b), it is obvious that the second control field ( $\Omega_d$ ) has significant influence on the structure of the transparency window (TW). The presence of the second control field makes the central portion of the TW

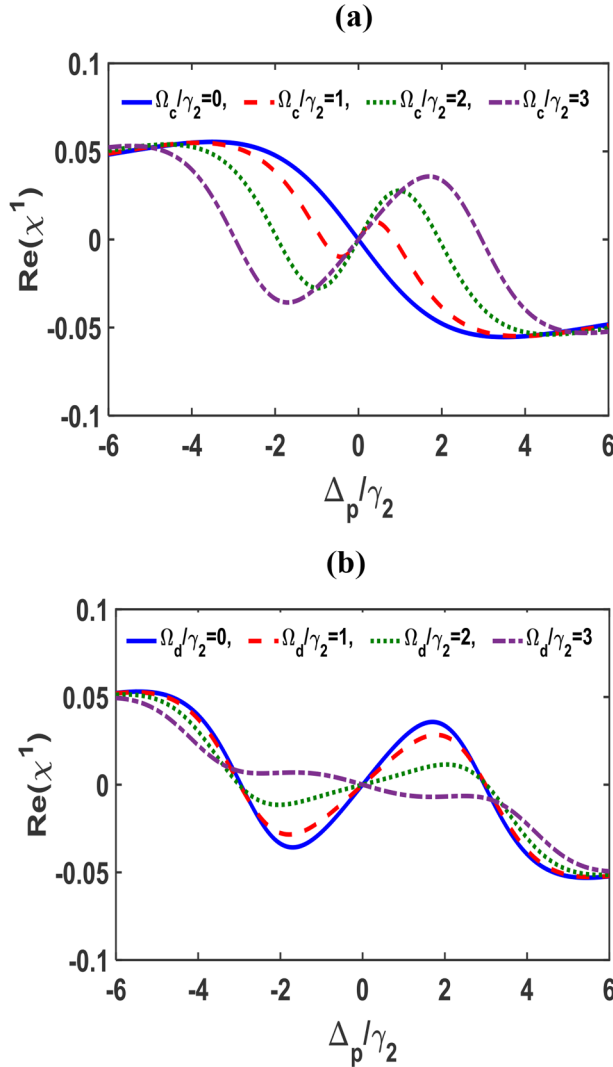


**Fig. 3.** Variations of real part of the linear susceptibility [ $\text{Re}(\chi^{(1)})$ ] with normalized probe detuning  $\Delta_p$ . (a) For different values of the first control field ( $\Omega_c$ ), while the second control field ( $\Omega_d$ ) is switched off. (b) For different values of the second control field ( $\Omega_d$ ), while keeping the value of first control field fixed ( $\Omega_c = 3 \text{ ps}^{-1}$ ). The value of detunings are  $\Delta_c = \Delta_d = 0$ .

almost uniform for certain values of  $\Omega_d$ .

We now proceed to examine the variation of real part of linear susceptibility  $\chi^{(1)}$  with the pump detuning frequency  $\Delta_p$  which has been depicted in Fig. 3. From Fig. 3(a), which depicts the variation of the real  $\chi^{(1)}$  in the absence of second control beam, it is evident that with the increase in the value of  $\Omega_c$ , the slope of the  $\chi^{(1)}$  gradually changes from a negative to positive value about the pump frequency (i.e.,  $\Delta_p = 0$ ). Since, the slope is related to the group velocity dispersion, this change signifies a shift from normal to anomalous dispersion regime. Note that a bright solitary wave can exist in a Kerr nonlinear medium provided that the medium exhibits anomalous dispersion. Fig. 3(b) demonstrates the variation of  $\text{Re}(\chi^{(1)})$  with the pump field detuning in presence of second control field (i.e., finite  $\Omega_d$ ). An interesting feature which emerges from careful examination of the profile of the  $\chi^{(1)}$  is that, the value of the slope of  $\chi^{(1)}$  in the neighbourhood of the pump frequency decreases with the increase in the value of  $\Omega_d$ . This implies in the neighbourhood of  $|\Delta_p| \leq 2$ , the medium will exhibit anomalous dispersion with small value which could be controlled by the second control field. Such medium could be very useful in some specific optoelectronic applications where small anomalous dispersion is desirable.

To this end, we examine the third order nonlinear susceptibility

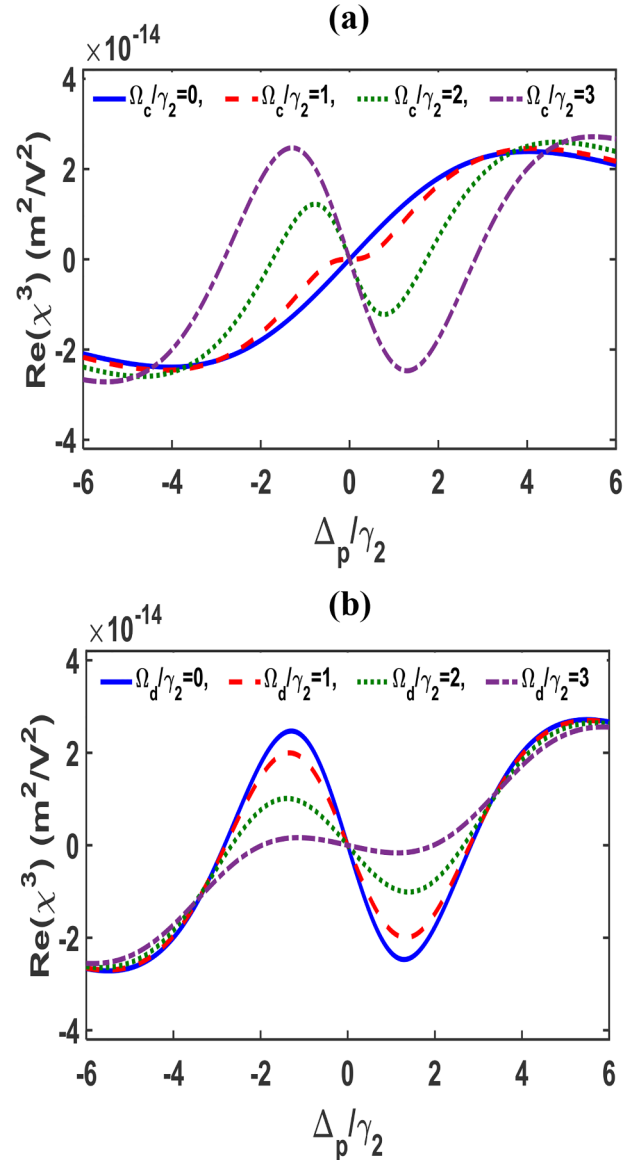


**Fig. 4.** Variations of real part of the Kerr nonlinearity [ $\text{Re}(\chi^{(3)})$ ] with normalized probe detuning. (a) For different values of the Rabi-frequency of the first control field ( $\Omega_c$ ), while the second control field ( $\Omega_d$ ) is switched off. (b) For different values of the Rabi-frequency of the second control field ( $\Omega_d$ ), while the value of the first control field has been kept constant ( $\Omega_c = 3 \text{ ps}^{-1}$ ). The value of detunings are  $\Delta_c = \Delta_d = 0$ .

which is related to the Kerr nonlinearity. At the outset, we have demonstrated the variation of the  $\text{Re}(\chi^{(3)})$  with the normalized probe detuning. Fig. 4 represents this variation when  $\Omega_d$  is switched off and on, respectively. The magnitude of the third order susceptibility is lowest when the detuning  $\Delta_p$  of the pump field is zero. However, the magnitude of the third order susceptibility increases with the increase in the value of the pump detuning. The sign of the third order nonlinearity can be changed by suitable choosing the value of the  $\Delta_p$ . Since, the sign of the Kerr nonlinearity and type of the dispersion are the deciding factors for the formation of bright and dark solitons, the detuning  $\Delta_p$  is a controlling parameter for the creation of these solitons.

We now investigate the property of the fifth order susceptibility  $\chi^{(5)}$  which is related to quintic nonlinearity by choosing appropriately suitable parameters. In Fig. 5 we have illustrated the variation of quintic nonlinearity with  $\Delta_p$  for different values of first and second control field Rabi-frequencies. From Fig. 5(a) it is seen that, for  $\Omega_c = 0$ , the profile of  $\chi^{(5)}$  shows anti-symmetric nature. For  $\Delta_p/\gamma_2 = 1$ ,  $\Omega_c/\gamma_2 = 2$ ,  $\Delta_c = 0$ , and

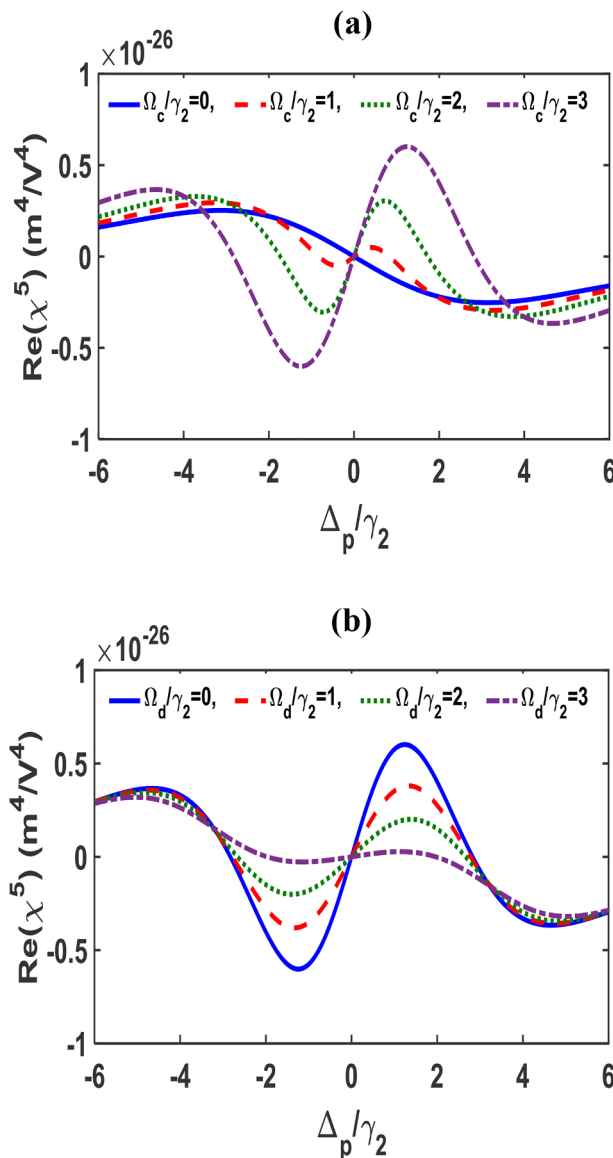


**Fig. 5.** Variations of real part of the quintic nonlinearity [ $\text{Re}(\chi^{(5)})$ ] with normalized probe detuning. (a) For different values of the Rabi-frequency of the first control field ( $\Omega_c$ ), while the second control field ( $\Omega_d$ ) is switched off. (b) For different values of the Rabi-frequency of the second control field ( $\Omega_d$ ), while keeping the value of the first control field fixed ( $\Omega_c = 3 \text{ ps}^{-1}$ ). The value of detunings are  $\Delta_c = \Delta_d = 0$ .

**Table 1**

Comparison of the typical values of quintic nonlinearities in quantum wells and other materials.

Material	$\chi^{(5)}$ in $\text{m}^4/\text{V}^4$	References
SiO <sub>2</sub> fiber	$-4.2 \times 10^{-38}$	[30]
As <sub>2</sub> Se <sub>3</sub> glass	$-1.29 \times 10^{-35}$	[31]
Metal colloids	$-1.37 \times 10^{-33}$	[32]
GaAs/Al <sub>0.2</sub> Ga <sub>0.8</sub> As quantum well	$0.25 \times 10^{-26}$	Present work

$\Omega_d = \Delta_d = 0$ , the typical value of  $\chi^{(5)}$  is  $0.25 \times 10^{-26} \text{ m}^4/\text{V}^4$  which is quite large. A comparison of the typical values of  $\chi^{(5)}$  in quantum wells and other materials have been given in Table 1 which clearly indicates existence of large quintic nonlinearity in coupled QWs. The magnitude of the fifth order nonlinearity in the neighbourhood of  $\Delta_p = 0$  is insignificant. However, with suitable choice of the value of controlling field, the

magnitude of fifth order nonlinearity can be enhanced within the transparency window (TW). Thus, the first control field acts as a controlling parameter. An additional control can be introduced by switching on the second control field, whose influence has been depicted in Fig. 5(b).

### Self-phase modulation in the coupled quantum well

We now adopt numerical simulation to investigate the self-phase modulation (SPM) owing to the existence of large optical nonlinearity. At the outset, we assume that only first control field is on and the second control field is off. We choose  $\Delta_p/\gamma_2 = -0.8$ ,  $\Delta_c/\gamma_2 = 2$ ,  $\Omega_c/\gamma_2 = 4$ , and  $\Omega_d = \Delta_d = 0$ . With the above choice of probe and control field parameters, the nonlinear coefficients associated with the Kerr and quintic nonlinearities turn out to be,  $\gamma = 1.16 \times 10^4 \text{ W}^{-1}\text{m}^{-1}$ , and  $\delta = -5.08 \times 10^3 \text{ W}^2\text{m}^{-1}$ , respectively. Values of other system parameters have been indicated in the previous section. In order to study self-phase modulation, we use Eq. (38), drop all dispersive terms, and introduce the transformation  $A(\xi, T) = \sqrt{P_0} Q(\xi, T)$ , to get the following equation:

$$i \frac{\partial Q}{\partial \xi} + \gamma P_0 |Q|^2 Q + \delta P_0^2 |Q|^4 Q = 0, \quad (39)$$

where,  $P_0$  and  $Q(\xi, T)$  represent peak power and form of the pulse, respectively. The solution of the above equation is  $Q(\xi, T) = Q(0, T) \exp(i\phi_{nl}(\xi, T))$ , where,  $\phi_{nl} = \xi \{ \gamma P_0 |Q(0, T)|^2 + \delta P_0^2 |Q(0, T)|^4 \}$  is the intensity dependent nonlinear phase shift. The frequency shift owing to this phase shift can be easily obtained using  $\omega(T) = -\frac{\partial \phi_{nl}}{\partial T}$ . Owing to the intensity dependent phase shift, new frequencies are generated as the pulse travels through the coupled QW system, and the intensity spectrum  $I(\omega)$  of the propagating pulse can be obtained using

$$I(\omega) = \left| \int_{-\infty}^{\infty} Q(\xi, T) \exp(i(\omega - \omega_0)T) dT \right|^2. \quad (40)$$

In order to examine self-phase modulation, we launch unchirped hyperbolic secant pulses  $A(\xi = 0, T) = \sqrt{P_0} Q(\xi = 0, T) = \sqrt{P_0} \operatorname{sech}(T/T_0)$  at the entrance of the coupled QW, where, the intensity full width at half maximum pulse duration is given by  $T_{FWHM} = 1.763 T_0$ . The temporal variations of frequency chirp at the end of the  $9.377 \mu\text{m}$  long coupled quantum well system for three different powers have been depicted in Fig. 6. The left panel represents spectral broadening due to Kerr nonlinearity alone, while the right panel represents broadening owing to both Kerr and quintic nonlinearities. Note-worthy important features are as follows: the SPM broadened spectra consist of multiple internal oscillations, and the number of these oscillations increases with the increases in the power of the pulse. The width of the broadened spectra increases with the increase in pulse peak power. Interestingly, in the presence of two control beams, the width of the broadened spectra increases with the increase in pulse peak power. The intensity of spectral lines decreases in presence of quintic nonlinearity, and this effect is very prominent at high power. Therefore, the quintic nonlinearity significantly reduces self-phase modulation (SPM). To examine the role of the second control beam ( $\Omega_d$ ) on self-phase modulation, the temporal variation of frequency chirp at the end of the QW system has been depicted in Fig. 7 for three different powers of the probe beam while, both control fields are switched on. Note the spectral behavior in the present case almost similar to the previous case, except one notable difference, in the present case the broadened spectra at different power levels is wider in comparing to the previous case. A noteworthy feature from Figs. 6 and 7 is the reduction in the amplitude of oscillations in the right panels. Note that the figures in the left panel are due to the Kerr nonlinearity alone, while that in the right panel is in the presence of both Kerr and quintic nonlinearities. The Kerr nonlinearity always increases with the increase in power of the optical beam, hence, the amplitude in the left panel of both figures increases with the increase in power. However, with the presence of quintic nonlinearity, the

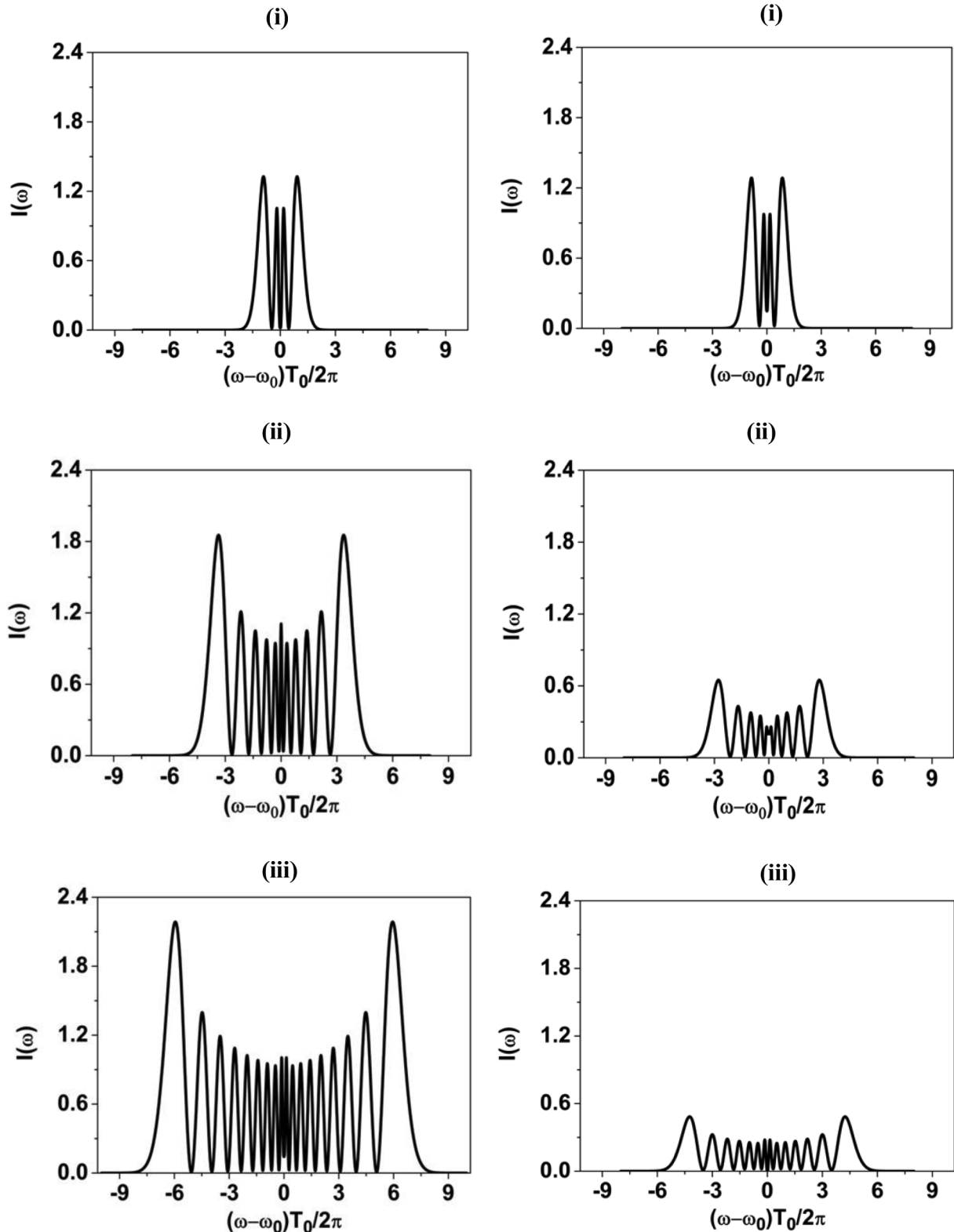


**Fig. 6.** The SPM broadened spectra of 500 fs pulses at the end of the multiple quantum well for the different powers, (i) 100, (ii) 300, (iii) 500 W of the probe pulse. Left panel is in absence of quintic nonlinearity, while the right panel is due to Kerr and quintic nonlinearities. Other relevant parameters are  $\Delta_p = -0.8\gamma_2$ ,  $\Delta_c = 2\gamma_2$ ,  $\Omega_c = 4\gamma_2$ ,  $\Omega_d = 0$ ,  $\Delta_d = 0$ ,  $\gamma = 1.16 \times 10^4 W^{-1} m^{-1}$ ,  $\delta = -5.08 \times 10^3 W^{-2} m^{-1}$ .

behavior of the overall nonlinearity of the system changes. The quintic part has a saturating influence in the total nonlinear response of the system. Owing to the presence of the quintic term, the magnitude of the total nonlinear response of the system decreases with the increase in the

power of the beam. Consequently, the amplitude in the right panel of Figs. 6 and 7 decreases with the increase in power. Another point to note is that the total energy of the pulse in the frequency and temporal domains must be conserved irrespective of cubic or quintic

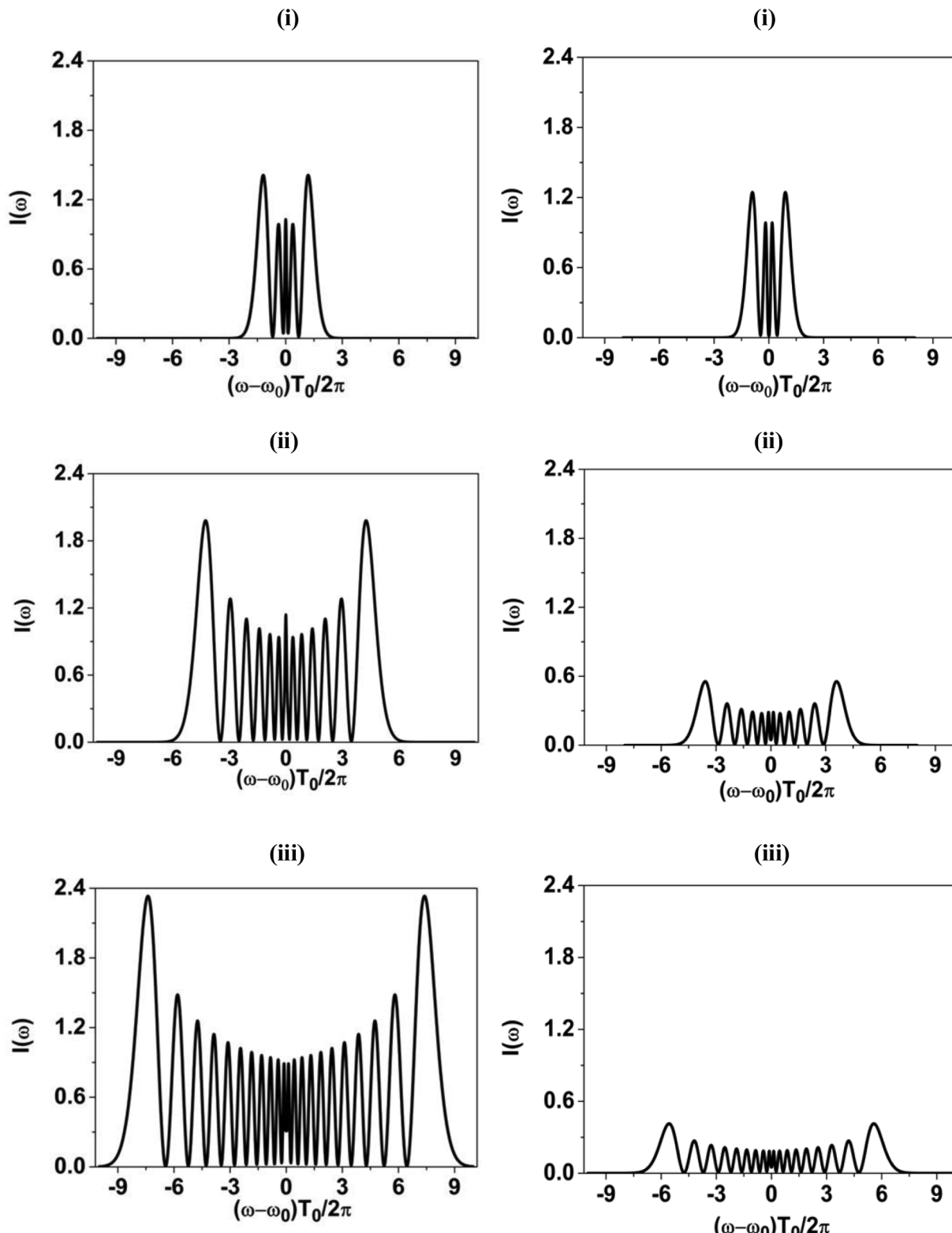


**Fig. 7.** The SPM broadened spectra of 500 fs pulses at the end of the multiple quantum well for the different powers (i) 100, (ii) 300, (iii) 500 W of the probe pulse. Left panel is in absence of quintic nonlinearity, while the right panel is due to Kerr and quintic nonlinearities. Other relevant parameters are  $\Delta_p = -0.8\gamma_2$ ,  $\Delta_c = 2\gamma_2$ ,  $\Omega_c = 4\gamma_2$ ,  $\Omega_d = 3\gamma_2$ ,  $\Delta_d = 2\gamma_2$ ,  $\gamma = 1.42 \times 10^4 W^{-1}m^{-1}$ ,  $\delta = -5.30 \times 10^3 W^{-2}m^{-1}$ .

nonlinearity. The area under the curves of left and right panels of Figs. 6 and 7 are not the same and hence, apparently they raise concern about the energy conservation in the frequency domain. However, a careful examination dispels this fear. What is being depicted in Figs. 6 and 7 are how the energy is redistributed over different frequencies in

the leading and trailing edges of the pulse. The redistributed energy is at the cost of energy which was available in the pump frequency. After redistribution of energy in the leading and trailing edges, the energy in the pump frequency decreases, which is not depicted in the figure. Therefore, it shall not be prudent to doubt energy conservation in the

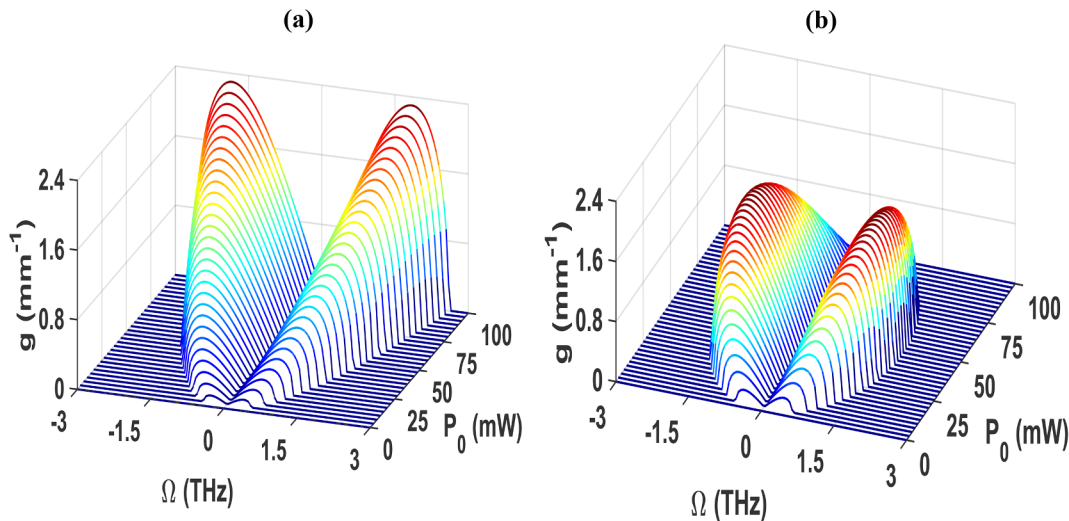


**Fig. 8.** Variation of MI gain with the frequency and power in absence of fourth order dispersion (i.e.,  $\Gamma_4=0$ ). (a) Only Kerr nonlinearity present. (b) Both Kerr and quintic nonlinearities are present.

frequency domain from Figs. 6 and 7. Note that the net energy loss by the pulse in the medium is zero. On the other hand, the issue of energy conservation in the temporal domain can be addressed by examination of the temporal shape of the pulse. The temporal shape of the pulse, as explained previously, is expressed as,  $A(\xi, T) = \sqrt{P_0} Q(\xi, T) = \sqrt{P_0} Q(0, T) \exp(i\phi_{nl}(\xi, T)) = A(0, T) \exp(i\phi_{nl}(\xi, T))$ , with  $P_0$  and  $Q(\xi, T)$  represent peak power and form of the pulse, respectively;  $A(0, T)$  is the initial profile of the pulse, while  $A(\xi, T)$  is the profile of the pulse after it has experienced self-phase modulation. Since  $|A(\xi, T)|^2 = |A(0, T)|^2$ , the temporal shape of an optical pulse does not change if it undergoes self-phase modulation. The energy of the pulse is always proportional to its temporal shape  $|A(\xi, T)|^2$ , hence, the energy of the optical pulses remains conserved after they experience SPM.

### Modulation instability of the probe beam

In this section we investigate modulation instability (MI) of a quasi-continuous or continuous wave (CW) probe beam using standard procedure [11,18,33]. The steady state solution of Eq. (38) is taken as:

$$A(\xi, T) = \{\sqrt{P_0} + a(\xi, T)\} \exp(i\{\gamma P_0 + \delta P_0^2\}\xi), \quad (41)$$

which leads to,

$$\frac{i\partial a}{\partial \xi} - \frac{1}{2!} \Gamma_2(0) \frac{\partial^2 a}{\partial T^2} - \frac{i}{3!} \Gamma_3(0) \frac{\partial^3 a}{\partial T^3} + \frac{1}{4!} \Gamma_4(0) \frac{\partial^4 a}{\partial T^4} + (\gamma P_0 + \delta P_0^2)(a + a^*) = 0, \quad (42)$$

where,  $\sqrt{P_0}$  and  $a(\xi, T)$  represent the amplitude of the CW and small perturbation in the steady state. The parameter  $a(\xi, T)$  consists of two side band plane waves of form,

$$a(\xi, T) = C \exp(i(K\xi - \Omega T)) + D \exp(-i(K\xi - \Omega T)), \quad (43)$$

where, C and D are amplitude of small perturbation. K and  $\Omega$  are wave number and frequency of the perturbation. By virtue of the Eq. (43), Eq. (42) yields following two homogenous equations of C and D:

$$C(-K + G) + \{(\gamma + 2\delta P_0)P_0\}D = 0, \quad (44)$$

$$\{(\gamma + 2\delta P_0)P_0\}C + (K + G)D = 0, \quad (45)$$

where,  $G = \frac{\Gamma_2(0)\Omega^2}{2!} + \frac{\Gamma_3(0)\Omega^3}{3!} + \frac{\Gamma_4(0)\Omega^4}{4!} \{(\gamma + 2\delta P_0)P_0\}$ , and  $G = \frac{\Gamma_2(0)\Omega^2}{2!} - \frac{\Gamma_3(0)\Omega^3}{3!} + \frac{\Gamma_4(0)\Omega^4}{4!} + \{(\gamma + 2\delta P_0)P_0\}$ . The nontrivial solution of the Eqs. (44) and (45) for the wave number leads to the dispersion relation:

$$K = \frac{1}{6} \Gamma_3 \Omega^3 \pm i \left[ \left( \Gamma_2 \Omega^2 + \frac{\Gamma_4 \Omega^4}{4!} \right) \{(\gamma + 2\delta P_0)P_0\} - \left( \frac{\Gamma_2 \Omega^2}{2!} + \frac{\Gamma_4(0) \Omega^4}{4!} \right)^2 \right]^{\frac{1}{2}}. \quad (46)$$

The gain of the modulation instability (MI) at frequency  $\Omega$  is given by,

$$g(\Omega) = 2 \times \text{Im}(K) = 2 \left[ \left( \Gamma_2 \Omega^2 + \frac{\Gamma_4 \Omega^4}{4!} \right) \{(\gamma + 2\delta P_0)P_0\} - \left( \frac{\Gamma_2 \Omega^2}{2!} + \frac{\Gamma_4(0) \Omega^4}{4!} \right)^2 \right]^{\frac{1}{2}}. \quad (47)$$

The instability gain maximizes at the critical frequency  $\Omega_c$  given by,

$$\Omega_c = \left[ 6 \left\{ \left( \frac{\Gamma_2}{\Gamma_4} \right)^2 + \frac{2 \{(\gamma + 2\delta P_0)P_0\}}{\Gamma_4} \right\}^{\frac{1}{2}} - 6 \frac{\Gamma_2}{\Gamma_4} \right]^{\frac{1}{2}}. \quad (48)$$

To the end, we first examine the modulation instability in absence of the second control beam (i.e.,  $\Omega_d = 0$ ). In order to do that we choose the probe detuning  $\Delta_p = -0.8\gamma_2$ ,  $\Omega_c = 2\gamma_2$  and  $\Delta_c = 0$ . The value of other relevant parameters are  $\gamma = 1.15 \times 10^4 W^{-1} m^{-1}$ ,  $\delta = -6.82 \times 10^3 W^{-2} m^{-1}$ ,  $\Gamma_2 = -6.80 \times 10^4 m^{-1} ps^2$ ,  $\Gamma_4 = 3.07 \times 10^5 m^{-1} ps^4$ . The instability gain as a function of perturbed frequency and probe beam power has been demonstrated in Fig. 8 in absence of the fourth order dispersion (i.e.,  $\Gamma_4=0$ ). In absence of the quintic nonlinearity, as evident from the left panel of the Fig. 8, gain as well as the band width of the gain increase with the increase in probe beam power  $P_0$ . However, in presence of quintic nonlinearity both gain and band width first increase with the power to attain a maximum value, then decreases with the increase in power and finally disappear above certain power. To examine the influence of the fourth order dispersion, we have demonstrated instability growth rate as a function of perturbed frequency and power of the probe beam in Fig. 9. From Fig. 9 it is evident that, irrespective of the presence of quintic nonlinearity the fourth order dispersion reduces growth considerably. Therefore, the system is less susceptible to modulation instability in presence of fourth-order dispersion.

We now proceed to investigate the effect of detuning ( $\Delta_c$ ) of the control field on the instability growth. The variations of the instability growth at different control field detunings have been depicted in Fig. 10. The upper and lower panels are in absence and presence of  $\Gamma_4$ , respectively. The growth is maximum when no control field detuning is present. As the value of  $\Delta_c$  increases, the growth rate of the instability as well as the bandwidth of frequencies susceptible to instability growth

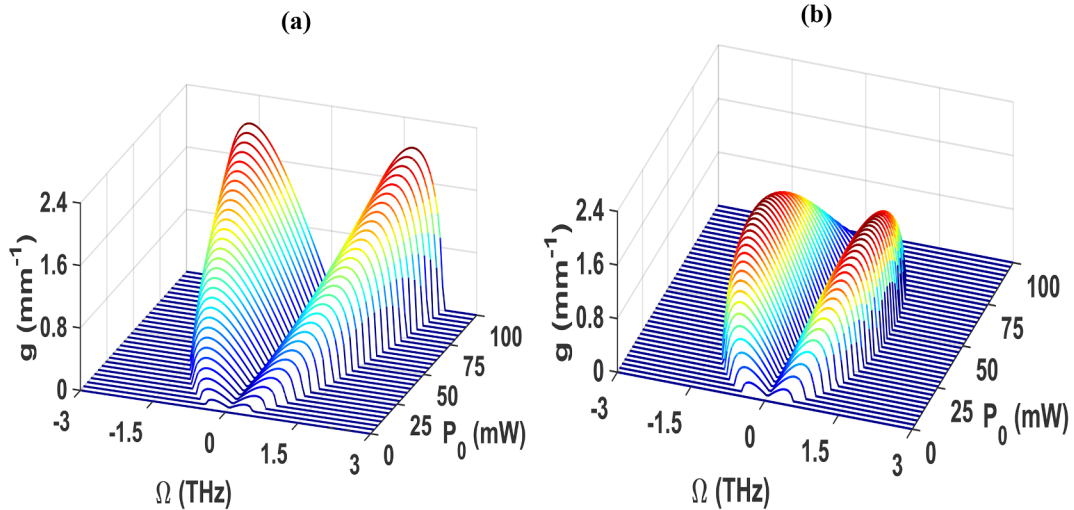


**Fig. 9.** Variation of MI gain with frequency and power in presence of fourth order dispersion (i.e.,  $\Gamma_4 \neq 0$ ). (a) Only Kerr nonlinearity present. (b) Both Kerr and quintic nonlinearities are present.

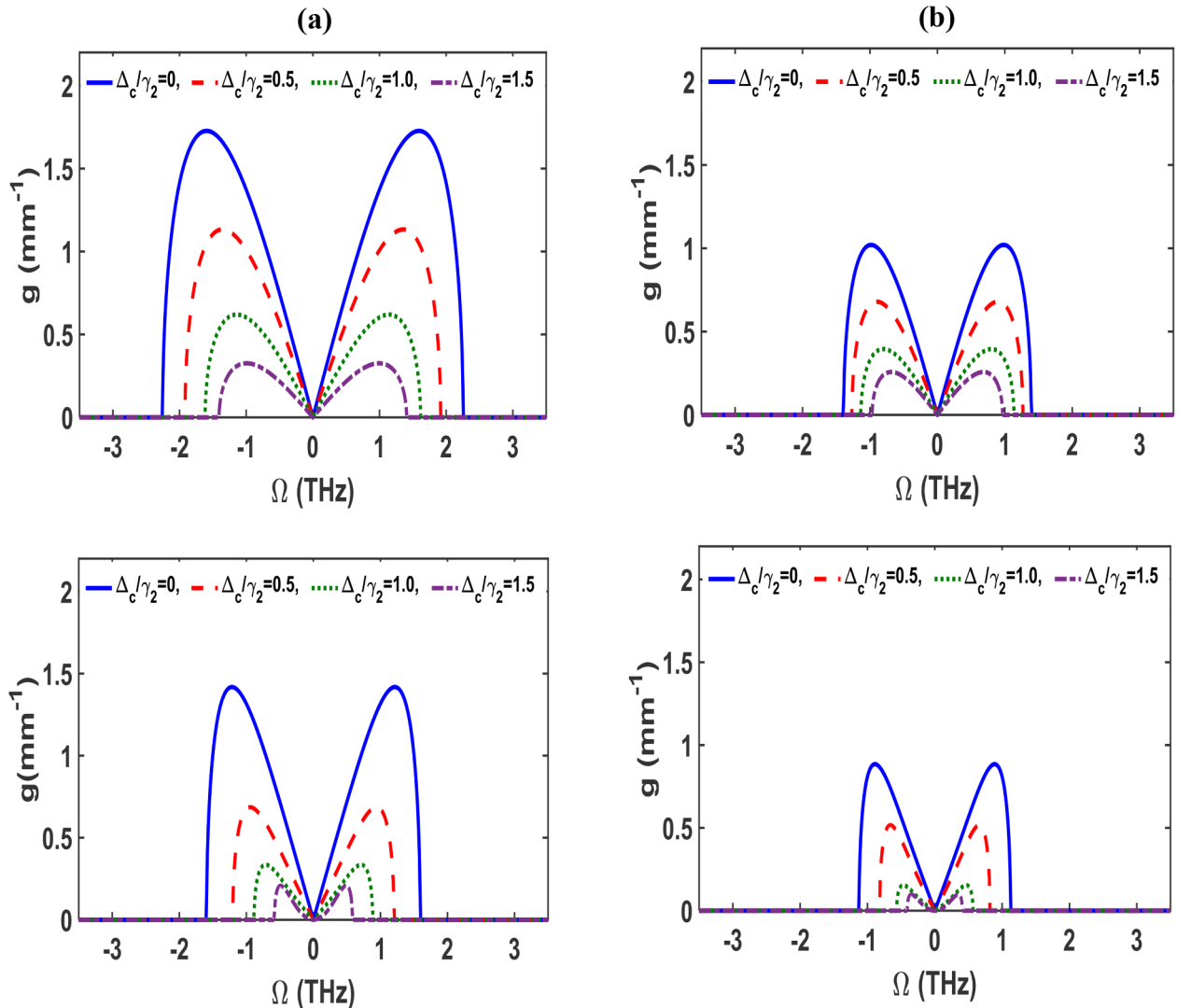


**Fig. 10.** Variations of MI gain with frequency at pump peak power  $P_0=75$  mW for different values of control field detuning  $\Delta_c$ . (a) Only Kerr nonlinearity present. (b) Both Kerr and quintic nonlinearities are present. In the upper panel  $\Gamma_4=0$ , while in the lower panel  $\Gamma_4$  is finite.

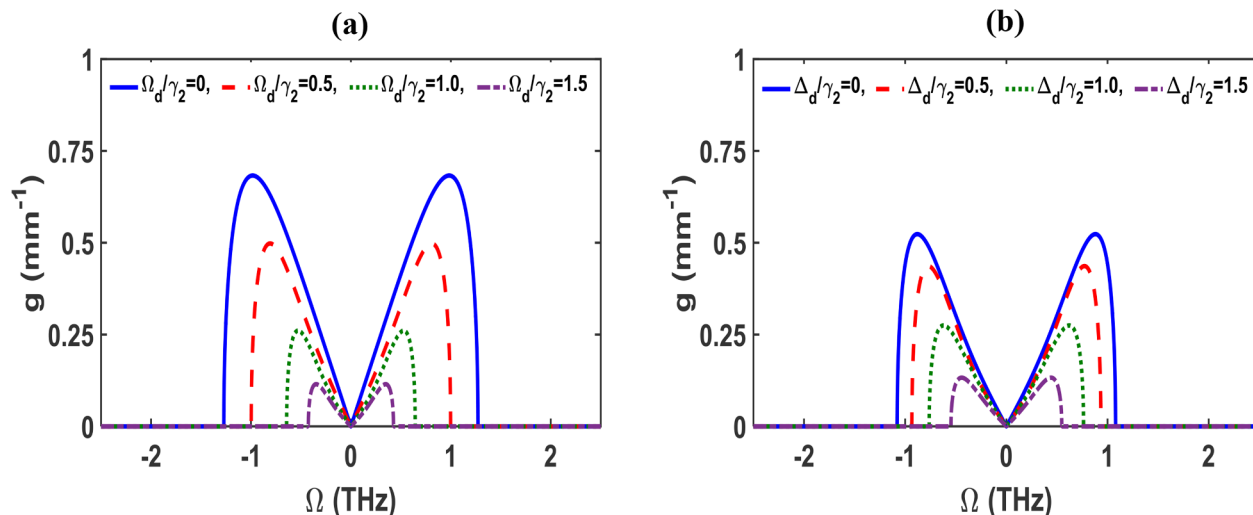


**Fig. 11.** Variations of MI gain with frequency in presence of both first and second control field. First control field Rabi frequency  $\Omega_c = 2\gamma_2$ , detuning  $\Delta_p = -0.8\gamma_2$ ,  $\Delta_c = 2\gamma_2$ ,  $\Delta_d = \gamma_2$ , probe beam peak power  $P_0 = 75$  mW. (a) At different values of second control Rabi frequency  $\Omega_d$ . (b) At different values of second control field detuning  $\Delta_d$ , while the values of  $\Omega_d = \gamma_2$ . Here in both panels  $\Gamma_4$  is finite.

decrease. This behavior remains unaffected irrespective of the value of fourth order dispersion.

To this end, we examine the effect of the second control field ( $\Omega_d$ ) on the modulation instability. The variation of the instability growth with frequency at a pump peak power  $P_0 = 75\text{mW}$  has been depicted in Fig. 11. The left panel indicates instability growth at different values of Rabi frequency of the second control field, while the right panel indicates instability growth at different detuning of the second control beam. From the left panel of Fig. 11, it is evident that, with the increase in the value of  $\Omega_d$ , the bandwidth of the frequency where the instability occurs decreases. Thus, a second control field decreases the bandwidth of instability gain where the system is susceptible to modulation instability. The right hand panel demonstrates the influence of the detuning of the second control field. Note that with the increase in the value of detunings, both bandwidth and instability growth decrease. The influence of the second control field is significant only when the frequency detuning  $\Delta_d = 0$ . With the increase in the value of detuning ( $\Delta_d$ ), growth as well as the bandwidth of frequencies decrease. Therefore, the influence of the second control field over the instability recedes with the increase in its frequency offset.

## Conclusion

In conclusion, we have identified large Kerr and quintic nonlinearities in asymmetric double quantum wells under the regime of electromagnetically induced transparency. The magnitude of these nonlinearities could be controlled by controlling the Rabi frequency and detuning of the controlling fields. A propagating probe pulse experiences self-phase modulation which is suppressed by the quintic nonlinearity. The intensity and width of the self-phase modulation spectra could be controlled by two control fields.

A propagating continuous wave or quasi-continuous probe beam undergoes modulation instability owing to the presence of large nonlinearities. The growth of the instability and bandwidth of unstable frequencies could be externally governed by the Rabi-frequency, two control detunings and power of the probe beam. Both fourth order dispersion and quintic nonlinearity reduce the growth and bandwidth of unstable frequencies.

## Conflict of Interest

All the authors have no conflict of Interest in this publication.

## CRediT authorship contribution statement

**Rohit Mukherjee:** Methodology, Software, Investigation, Data curation, Writing - original draft, Funding acquisition. **S. Konar:** Conceptualization, Validation, Writing - review & editing, Funding acquisition, Project administration, Supervision.

## Acknowledgments

We thank anonymous reviewers for helpful suggestion. Defense research and Development organization (DRDO), New Delhi, Government of India, has supported the investigation through the project ERIP/ER/1202225/M/01/1668. The authors thank DRDO for the support. One of the author RM thank N. Borgohain for valuable discussions and suggestions.

## References

- [1] Hang C, Li Y, Ma L, Huang G. Three-way entanglement and three qubit phase gate based on a coherent six level atomic system. *Phys Rev A* 2006;74:012319. <https://doi.org/10.1103/PhysRevA.74.012319>.
- [2] Wu J-H, Gao J-Y, Xu J-H, Silvestri L, Artoni M, La Rocca G C, et al. Ultrafast all optical switching via tunable Fano interference. *Phys Rev Lett* 2005;95:057401. <https://doi.org/10.1103/PhysRevLett.95.057401>.
- [3] Kang H, Hernandez G, Zhu Y. Slow-light six-wave mixing at low intensities. *Phys Rev Lett* 2004;93:073601. <https://doi.org/10.1103/PhysRevLett.93.073601>.
- [4] Felinto D, Moretti D, de Oliveira RA, Tabosa JWR. Delayed four-and six wave mixing in a coherently prepared atomic ensembles. *Opt Lett* 2010;35:3937–9. <https://doi.org/10.1364/OL.35.003937>.
- [5] Frogley MD, Dynes JF, Beck M, Faist J, Philips CC. Gain without inversion in semiconductor nanostructures. *Nat Mater* 2006;5:175–8. <https://doi.org/10.1038/nmat1586>.
- [6] Dynes JF, Frogley MD, Rodger J, Philips CC. Optically mediated coherent population trapping in asymmetric semiconductor quantum wells. *Phys Rev B* 2005;72:085323–85327. <https://doi.org/10.1103/PhysRevB.72.085323>.
- [7] Marangos JP. Electromagnetically induced transparency. *J Mod Opt* 1998;45:471–503. <https://doi.org/10.1080/09500349808231909>.
- [8] Fleischhauer M, Imamoglu A, Marangos JP. Electromagnetically induced transparency: optics in coherent media. *Rev Mod Phys* 2005;77:633–73. <https://doi.org/10.1103/RevModPhys.77.633>.
- [9] Wang WX, Hou JM, Lee RK. Ultraslow bright and dark solitons in semiconductor quantum wells. *Phys Rev A* 2008;77. <https://doi.org/10.1103/PhysRevA.77.033838>.
- [10] Zhu C, Huang H. Slow-light solitons in coupled asymmetric quantum wells via interband transitions. *Phys Rev B* 2009;80:235408. <https://doi.org/10.1103/PhysRevB.80.235408>.
- [11] Shwetashumala S, Konar S, Biswas A. Ultraslow solitons due to large quintic nonlinearity in coupled quantum well structure driven by two control laser beams. *Appl Phys B* 2013;111:53–64. <https://doi.org/10.1007/s00340-012-5306-0>.
- [12] Niu Y, Gong S, Li R, Xu Z, Liang X. Giant Kerr nonlinearity induced by interacting

- dark resonances. Opt Lett 2005;30:3371–3. <https://doi.org/10.1364/OL.30.003371>.
- [13] Yang XX, Li Z-w, Wu Y. Four-wave mixing via electron spin coherence in a quantum well waveguide. Phys Lett A 2005;340:320–5. <https://doi.org/10.1016/j.physleta.2005.04.019>.
- [14] Borgohain N, Belir M, Konar S. Giant parabolic nonlinearities at infrared in  $\Lambda$ -type three level multiple quantum wells. Annal Phys 2015;361:107–19. <https://doi.org/10.1016/j.aop.2015.06.006>.
- [15] Zhu C, Huang G. Giant Kerr nonlinearity controlled entangled photons and polarization phase gates in coupled quantum-well structures. Opt Exp 2011;19:23364–76. <https://doi.org/10.1364/OE.19.023364>.
- [16] Wang WX, Zha TT, Lee RK. Giant Kerr nonlinearities and slow optical solitons in coupled double quantum-well nanostructure. Phys Lett A 2009;374:355–9. <https://doi.org/10.1016/j.physleta.2009.11.002>.
- [17] Borgohain N, Belir M, Konar S. Infrared supercontinuum generation in multiple quantum well nanostructures. J Opt 2016;18:115001. <https://doi.org/10.1088/2040-8978/18/11/115001>.
- [18] Borgohain N, Konar S. The effects of control field detuning on the modulation instability in a three-level quantum well system. J Appl Phys 2016;119:213103. <https://doi.org/10.1063/1.4953005>.
- [19] Terzis AF, Kosionis SG, Boviatissis J, Paspalakis E. Nonlinear optical susceptibilities of semiconductor quantum dot – metal nanoparticle hybrids. J Mod Opt 2015;63:451–61. <https://doi.org/10.1080/09500340.2015.1079655>.
- [20] Peng Y, Yang A, Chen B, Xu Y, Hu X. Tunneling-induced large fifth-order nonlinearity with competing linear and nonlinear susceptibilities. J Opt Soc Am B 2014;31:2188–92. <https://doi.org/10.1364/JOSAB.31.002188>.
- [21] Zubairy MS, Matsko AB, Scully MO. Resonant enhancement of high-order optical nonlinearities based on atomic coherence. Phys Rev A 2002;65:043804. <https://doi.org/10.1103/PhysRevA.65.043804>.
- [22] Giri DK, Gupta PS. Short time squeezing effects in spontaneous and stimulated six-wave mixing process. Opt Commun 2003;221:135–413. [https://doi.org/10.1016/S0030-4018\(03\)01464-0](https://doi.org/10.1016/S0030-4018(03)01464-0).
- [23] Zhang Y, Khadka U, Anderson B, Xiao M. Temporal and spatial interference between four-wave mixing and six-wave mixing. Phys Rev Lett 2009;102:013601. <https://doi.org/10.1103/PhysRevLett.102.013601>.
- [24] Greenberg JA, Gauthier DJ. High-order optical nonlinearity at low light levels. Europhys Lett 2012;98:24001. <https://doi.org/10.1209/0295-5075/98/24001>.
- [25] Roskos HG, Nuss MC, Shah J, Leo K, Miller DAB, Fox AM, et al. Coherent submillimeter-wave emission from charge oscillations in a double-well potential. Phys Rev Lett 1992;68:2216–9. <https://doi.org/10.1103/PhysRevLett.68.2216>.
- [26] Luo XQ, Wang DL, Zhang ZQ, Ding JW, Liu WM. Nonlinear optical behaviour of a four level quantum well with coupled relaxation of optical and longitudinal phonons. Phys Rev A 2011;84:033803. <https://doi.org/10.1103/PhysRevA.84.033803>.
- [27] Scully MO, Zubairy MS. Quantum optics. Cambridge: Cambridge University Press; 2001.
- [28] Wu Y, Deng L. Ultraslow optical solitons in a cold four-state medium. Phys Rev Lett 2004;93:143904. <https://doi.org/10.1103/PhysRevLett.93.143904>.
- [29] Wu Y, Deng L. Ultraslow bright and dark optical solitons in a cold three state medium. Opt Lett 2004;29:2064–6. <https://doi.org/10.1364/OL.29.002064>.
- [30] Pushkarov D, Tanev S. Bright and dark solitary wave propagation and bistability in the anomalous dispersion region of optical waveguide with third and fifth order nonlinearities. Opt Commun 1996;124:354–64. [https://doi.org/10.1016/0030-4018\(95\)00552-8](https://doi.org/10.1016/0030-4018(95)00552-8).
- [31] Boudebs G, Cherukulappurath S, Leblond H, Troles J, Smekta F, Sanchez F. Experimental and theoretical study of higher-order nonlinearities in chalcogenide glasses. Opt Commun 2003;219:427–33. [https://doi.org/10.1016/S0030-4018\(03\)01341-5](https://doi.org/10.1016/S0030-4018(03)01341-5).
- [32] Reyna AS, de Araújo CB. Spatial phase modulation due to quintic and septic nonlinearities in metal colloids. Opt Exp 2014;22:22456–69. <https://doi.org/10.1364/OE.22.022456>.
- [33] Sarma AK, Saha M. Modulational instability of coupled nonlinear field equations for pulse propagation in a negative index material embedded into a Kerr medium. J Opt Soc Am B 2011;28:944–8. <https://doi.org/10.1364/JOSAB.28.000944>.